Hydrol. Earth Syst. Sci. Discuss., 11, 1967–2009, 2014
www.hydrol-earth-syst-sci-discuss.net/11/1967/2014/
doi:10.5194/hessd-11-1967-2014

Hydrology and Earth System Sciences
Open Access
Discussions

Characterizing coarse-resolution watershed soil moisture heterogeneity using fine-scale simulations

W. J. Riley[1] **and C. Shen**[2]

[1]Earth Systems Division, Climate and Carbon Department, Lawrence Berkeley National Laboratory, Berkeley, CA 94720, USA
[2]Department of Civil and Environmental Engineering, 206C Sackett Building, The Pennsylvania State University, University Park, PA 16802, USA

Received: 12 November 2013 – Accepted: 25 January 2014 – Published: 11 February 2014

Correspondence to: W. J. Riley (wjriley@lbl.gov)

Published by Copernicus Publications on behalf of the European Geosciences Union.

Abstract

Watershed-scale hydrological and biogeochemical models are usually discretized at resolutions coarser than where significant heterogeneities in topographic, subsurface abiotic and biotic, and surface vegetation exist. Here we report on a method to use fine-resolution (220 m gridcells) hydrological model predictions to build reduced order models of the statistical properties of near-surface soil moisture at coarse-resolution (2^5 times coarser; ~ 7 km). We applied a watershed-scale hydrological model (PAWS+CLM) that has been previously tested in several watersheds and developed simple, relatively accurate ($R^2 \sim 0.7$–0.8) reduced order models for the relationship between mean and higher-order moments of near-surface soil moisture during the non-frozen periods over five years. When applied to transient predictions, soil moisture variance and skewness were relatively accurately predicted ($R^2 \sim 0.7$–0.8), while the kurtosis was less accurately predicted ($R^2 \sim 0.5$). We tested sixteen system attributes hypothesized to explain the negative relationship between soil moisture mean and variance toward the wetter end of the distribution and found that, in the model, 59 % of the variance of this relationship can be explained by the elevation gradient convolved with mean evapotranspiration. We did not find significant relationships between the time rate of change of soil moisture variance and covariances between mean moisture and evapotranspiration, drainage, or soil properties, as has been reported in other modeling studies. As seen in previous observational studies, the predicted soil moisture skewness was predominantly positive and negative in drier and wetter regions, respectively. In individual coarse-resolution gridcells, the transition between positive and negative skewness occurred at a mean soil moisture of ~ 0.25–0.3. The type of numerical modeling experiments presented here can improve understanding of the causes of soil moisture heterogeneity across scales, and inform the types of observations required to more accurately represent unresolved spatial heterogeneity in regional and global hydrological models.

HESSD
11, 1967–2009, 2014

1 Introduction

Representation of the structure and dynamics of fine-scale spatial structure in hydrological states and fluxes has been shown to significantly influence coarse-scale surface energy budgets (e.g., ET, Vivoni et al., 2007; Wood, 1997, 1998), runoff and streamflow (Arrigo and Salvucci, 2005; Barrios and Frances, 2012; Vivoni et al., 2007), regional-scale feedbacks with the atmosphere (Nykanen and Foufoula-Georgiou, 2001), and biogeochemical responses (Dai et al., 2012; Zhang et al., 2012). It has been argued that the relevant spatial scale for hydrological state and flux heterogeneity is on the order of 10 m^2 (Wood et al., 2011), while for biogeochemical dynamics it may be as small as 1 m^2 (Burt and Pinay, 2005; Frei et al., 2012; Groffman et al., 2009; McClain et al., 2003). The current suite of land models representing coupled hydrological and biogeochemical cycles and used for analyses of water resources and water quality (e.g., HydroGeoSphere, Li et al., 2008; CATHY, Weill et al., 2011; PIHM, Qu and Duffy, 2007; tRibs, Ivanov et al., 2004; Noah-MP+CATHY, Niu et al., 2013; GSFlow, Markstrom et al., 2008; LEAF-Hydro-Flood, Miguez-Macho and Fan, 2012; GEOtop, Rigon et al., 2006; MIKE-SHE, McMichael et al., 2006; WEP-L, Jia et al., 2006, and PAWS, Shen, 2009; Shen and Phanikumar, 2010), and regional (e.g., Subin et al., 2011) and global (e.g., Koven et al., 2013; Tang et al., 2013) climate prediction are typically applied at resolutions that are orders of magnitude larger than these scales. Unfortunately, there are few large-scale observational datasets with which to test the impact of the discrepancies in scale between model representation and known variability of coupled hydrological and biogeochemical processes. This problem is particularly acute for biogeochemical dynamics, which generally depend strongly on the hydrological state.

Watershed-scale hydrological models are often tested against, or calibrated to, stream flow observations. The impact of these types of calibrations on the relative accuracy of surface soil moisture heterogeneity is not well characterized. For example, Nykanen and Foufoula-Georgiou (2001) used observations form the 1997 SGP experiment to investigate the impact of nonlinear soil moisture dependencies of parameters

HESSD
11, 1967–2009, 2014

on the scale dependency of those parameters. They showed that failing to consider this scale dependency could cause large biases in predicted surface runoff. Gebremichael et al. (2009) compared scaling characteristics of spatial soil moisture fields from the same 1997 SGP experiment with predicted values from a distributed hydrologic model. Inconsistencies between the observed and predicted soil moisture mean and spatial scaling parameters indicated that while the model accurately reproduced outlet stream flow the underlying mechanisms leading to runoff might have been inaccurately simulated.

Quantifying relationships between the statistical properties of the soil moisture field and spatial scale may allow prediction of heterogeneity at scales finer than those resolved by the model. Since the pioneering work of Rodriguez-Iturbe (1995) and Wood (1998), who described the power law decay of variance as a function of the observation scale, many studies have quantified the variance-scale relationship. Hu et al. (1997) showed that the variance (σ_θ^2) of the soil moisture (θ) field at different spatial averaging areas (A) can be related to the ratio of those areas raised to a scaling exponent (γ; i.e., "simple scaling"). They also showed that γ is related to the spatial correlation structure of the soil moisture field and that it decreases as soils dry. Their scaling analysis of higher-order moments indicated that soil moisture might not always follow simple scaling. A number of investigators have since demonstrated that the relationship between σ_θ^2 and spatial scale is not log-log linear across all spatial scales, and that the relationship can depend on the soil moisture (μ_θ) field (e.g., Das and Mohanty, 2008; Famiglietti et al., 1999; Joshi and Mohanty, 2010; Mascaro et al., 2010, 2011; Nykanen and Foufoula-Georgiou, 2001).

It has been further observed that soil moisture mean is often related to its variance and higher-order moments. Most commonly, an upward convex relationship between μ_θ and σ_θ^2 has been reported when a sufficiently large range of mean moistures is analyzed (e.g., Brocca et al., 2010, 2012; Choi and Jacobs, 2011; Famiglietti et al., 2008; Lawrence and Hornberger, 2007; Li and Rodell, 2013; Pan and Peters-Lidard, 2008; Rosenbaum et al., 2012; Tague et al., 2010; Teuling and Troch, 2005; Teuling

HESSD
11, 1967–2009, 2014

et al., 2007). Theoretical analyses have indicated that an upward convex relationship is consistent with current understanding of soil moisture dynamics (e.g., Vereecken et al., 2007).

Famiglietti et al. (2008) used over 36 000 soil moisture observations in four field campaigns to demonstrate that soil moisture variability generally increased with extent scale and followed fractal scaling. Their reported soil moisture standard deviation vs. mean moisture content exhibited a convex upward relationship, with the peak of their best-fit relationships occurring at ~ 0.15 mean soil moisture. Brocca et al. (2012), using data from 46 sites over two years in two adjacent ~ 200 km^2 areas, observed a peak in the convex upward relationship around 0.2–0.25 mean soil moisture. Choi and Jacobs (2011) studied observations from two years of the Walnut Creek watershed, Iowa, Soil Moisture Experiment (2002, 2005). They observed a convex upward relationship during the 2002 observations when the soil moisture range extended down to ~ 0.1, but not in 2005 when mean soil moisture did not drop below ~ 0.15. Rosenbaum et al. (2012) concluded that the relationship between the 0–5 cm soil moisture spatial standard deviation and mean also had a convex up shape, but peaked at a higher mean soil moisture (0.35–0.40), although their range of soil moisture extended substantially further (0.58) than the other studies cited above.

Several studies have also investigated the relationships between observed soil moisture mean and higher order moments (skewness (s_θ) and kurtosis (k_θ)). For example, Famiglietti et al. (1999) used observations from the SGP97 experiment to conclude that the distribution of surface moisture content evolved from negatively skewed under very wet conditions, to uniform in the midrange of mean moisture, to positively skewed under dry conditions. For the same SGP97 dataset, Ryu and Famiglietti (2005) discussed the bimodality of the soil moisture distributions (which will be reflected in k_θ), and concluded that it resulted primarily from fractional precipitation within the observational footprint.

A fewer number of studies have combined observations of soil moisture with distributed hydrological model predictions to investigate spatial scaling properties. Li and

HESSD
11, 1967–2009, 2014

Rodell (2013) examined spatial statistics of in situ, satellite-retrieved, and modeled soil moisture over three large climate regions. The relationship between σ_θ^2 and μ_θ had an upward convex shape for the in situ measurements, but not for the modeled relationship. Manfreda et al., 2007 examined the statistical structure of soil moisture patterns using modeled soil moisture obtained from the North American Land Data Assimilation System (NLDAS). They concluded that σ_θ^2 followed a power law relationship with averaging area and the dynamics of the relationship were controlled by mean soil water content. Maxwell (2010) performed transient simulations of an arid mountain system and showed that the land-energy fluxes were spatially correlated and that the soil saturation vertical structure did not follow a simple scaling relationship. Ivanov et al. (2010) studied the relationship between soil moisture mean and its coefficient of variation using a numerical model applied to a small hillslope, and demonstrated hysteretic patterns during the wetting-drying cycle. They concluded that the system response is not unique given the same initial mean state, but that it depends on the magnitude of precipitation inputs and the triggering of subsurface lateral flow.

The relationships between soil moisture mean and statistical moments potentially depend on a wide range of factors and on spatial extent. As reviewed in Brocca et al. (2007), soil moisture statistical properties can be impacted by lateral redistribution (Moore et al., 1988; Williams et al., 2003), radiation (Moore et al., 1993; Western et al., 1999), soil characteristics (Famiglietti et al., 1998; Hu et al., 1997; Seyfried, 1998), vegetation characteristics (Hupet and Vanclooster, 2002; Qiu et al., 2001), elevation above the drainage channel (Crave and GascuelOdoux, 1997), downslope gradient (Merot et al., 1995), bedrock topography (Chaplot and Walter, 2003), specific upslope area (Brocca et al., 2007), and landscape unit (Park and van de Giesen, 2004; Wilson et al., 2004). Famiglietti et al. (1998) argued that under wet conditions, the best correlation of soil moisture variability was with soil porosity and hydraulic conductivity, and under dry conditions, with relative elevation, aspect, and clay content. Western et al. (1999) found that during wet conditions the best predictor of the soil moisture spatial pattern was the

HESSD
11, 1967–2009, 2014

specific area (through lateral redistribution) while during dry conditions the best predictor was the potential solar radiation index (through aspect and evapotranspiration).

Albertson and Montaldo (2003) and Montaldo and Albertson (2003) presented a theoretical argument for the impact of various factors on the relationship between soil moisture mean and variance. They showed that covariances between anomalies of soil moisture, infiltration, drainage, and ET control the production and destruction of variance over time. Teuling and Troch (2005) applied a similar approach to study the impacts of vegetation, soil properties, and topography on the controls of soil moisture variance.

Extrapolating from the previous studies, we hypothesize that μ_θ and its higher-order moments follow (possibly complex) quantifiable relationships that can be used to understand controls on moisture heterogeneity and to better represent subgrid-scale moisture heterogeneity in watershed to regional-scale models. In the current approach, we begin with a downscaling hypothesis that consistent relationships between the transient higher-order statistical moments and mean near-surface soil moisture fields exist (i.e., a "downscaling" closure relationship). We leave the problem of upscaling these relationships and their impact on the coarse-resolution transient solution for further work. In particular, we used a five-year, high-resolution hydrological simulation of the Clinton River Watershed in Michigan to characterize relationships between μ_θ and σ^2_θ, s_θ, and k_θ. Although we expected these relationships to vary with depth, we only evaluated the depth interval 0–10 cm to make the analysis scope tractable; future work will address this shortcoming. We also tested the extent to which using discrete bins across the mean moisture range improved characterization of spatial soil moisture heterogeneity. We then applied these relationships to investigate hypothesized controllers of soil moisture heterogeneity as a function of soil properties, evapotranspiration, topography, etc.

In the Methods section we describe the Clinton River Watershed, the numerical model we applied (PAWS+CLM), model forcing and surface characterization, simulations performed, and our approach to generating a surrogate model of fine-scale soil

HESSD
11, 1967–2009, 2014

moisture heterogeneity. In Sect. 3 we discuss the ROM estimates, the value of using a binned approach to characterizing soil moisture variability, and predicted controls on the relationship between soil moisture mean and variance. The last section provides a brief summary and conclusions.

2 Methods

2.1 The Clinton River watershed

Our study domain is the Clinton River watershed (Fig. 1), an 1837 km^2, humid continental-climate basin draining into Lake St. Clair that was described in detail by Shen et al. (2013c). Precipitation is relatively uniformly distributed throughout the year but there is strong seasonal variation in solar radiation and air temperature that affect evapotranspiration (ET). The basin has rugged hills on the highlands of the west and flat, low-lying plains toward the east. Urban areas of varying intensity span the southern portion of the watershed, the northwest is largely forested, and the northeast is dominated by agriculture. Glacial drifts and lucastrine deposits in the southeast form the unconfined aquifer, underlain by shale rock that bears little water. High-resolution elevation (30 m), land use (30 m), soil (1 : 12 000 to 1 : 63 360 SSURGO), river hydrography (1 : 24 000), well-log based aquifer characteristics (~ 1000 m), land-based climate forcing data (12 stations; precipitation, temperature, humidity, and wind speeds), and simulated steady state carbon and nitrogen states (220 m) are used as inputs to the model (Shen et al., 2013c).

2.2 PAWS+CLM model description and simulations performed

We applied the PAWS+CLM model to generate watershed-scale predictions for the analyses presented here. PAWS (Process-based Adaptive Watershed Simulator) (Shen et al., 2013c; Shen and Phanikumar, 2010) is a computationally efficient, physically-based hydrologic model that has recently been coupled with CLM4.0

HESSD
11, 1967–2009, 2014

(Lawrence et al., 2011). PAWS+CLM explicitly solves the physically based governing PDEs for overland flow, channel flow, subsurface flow, wetlands, and the dynamic two-way interactions among these components. The model evaluates the integrated hydrologic response of the surface–subsurface system using a novel non-iterative method that couples runoff and groundwater flow to vadose zone processes approximating the three-dimensional (3-D) Richards equation. By reducing the dimensionality of the 3-D subsurface problem, the model significantly reduces the computational demand with little loss of physics representation.

The PAWS+CLM model has been tested extensively with analytical and 3-D benchmarks and compares favorably with other physically-based models (Maxwell et al., 2012). It has been applied in several US Midwest watersheds, including the 1140 km^2 Red Cedar River (Shen and Phanikumar, 2010), the 1837 km^2 Clinton River (Shen et al., 2013c), the 4527 km^2 Upper Grand (Shen et al., 2013b), the 5232 km^2 Kalamazoon River (Niu and Phanikumar, 2012), the 14 430 km^2 Grand River, and the 22 260 km^2 Saginaw River (Niu et al., 2011) basins. More recently, physically-based reactive transport of nutrients and bacteria has been integrated (Niu and Phanikumar, 2012) and the model has been applied to a desert environment in Southern California to evaluate groundwater sustainability (Shen et al., 2013a).

We applied PAWS+CLM at fine (220 m × 220 m) and coarse (7040 m × 7040 m) horizontal resolutions across the Clinton watershed. Vertical resolution (20 layers in the vadose zone) was constant across all grid cells. The simulations were performed from 2001 to 2008 with the first three years used as model "spin-up" and 2004–2008 included in our analysis. We used daily-averaged top 10 cm soil moisture (θ) fields for the analyses presented here. To simplify this first attempt at estimating quantitative relationships between the spatial properties of the fine-resolution moisture fields and the mean moisture fields, we focused on the unfrozen periods during each year (days 130–300). The 2004–2008 temporal average soil moisture predicted in the 220 m^2 simulation is shown in Fig. 1. There is a large-scale spatial pattern in the soil moisture field, being generally higher on the eastern lowland plains than on the western hills, due to

HESSD
11, 1967–2009, 2014

basin-scale groundwater flow. However, contrary to the coarse-resolution soil moisture map provided previously (Fig. 10d in Shen et al., 2013c), Fig. 1 shows fine-scale features, e.g., high surface moisture near channels and high moisture in clayey soils near the eastern boundary.

2.3 Developing surrogate models for surface soil moisture moments

We developed two classes of simple surrogate models to represent soil moisture spatial heterogeneity as a function of mean soil moisture in coarse-resolution gridcells. We chose a factor of 2^5 decrease in resolution to define the coarse-resolution gridcells, resulting in thirty-four 7040 m coarse-resolution gridcells across the watershed. The first class of surrogate model was separate polynomials describing the relationships between μ_θ and σ^2_θ, s_θ, and k_θ for each coarse-resolution gridcell. We tested the impact on the accuracy of the relationship for best-fit 1st, 2nd, and 3rd order polynomials. The second class of surrogate models represents the fraction of high-resolution gridcells in each coarse-resolution gridcell that fall into a particular soil-moisture bin. A disadvantage of this latter approach is that it is not as easy to mathematically synthesize the patterns, while a potential advantage is that it represents the probability distribution function of the moisture even in the case where the first few statistical moments do not fully capture its properties.

2.4 Relationships between soil moisture heterogeneity and system properties

We investigated the relationship between daily-average σ^2_θ and μ_θ over the μ_θ range where σ^2_θ decreases with increasing μ_θ. As shown below, most of the μ_θ predictions were above the ~ 0.2 breakpoint (as often observed and predicted here) for the peak of a convex-up relationship between σ^2_θ and μ_θ. Therefore, many of the coarse-resolution gridcells were relatively well characterized by a linear fit with a negative slope, although about 20 % of the gridcells were predicted to have a convex-up relationship. For the

HESSD
11, 1967–2009, 2014

latter gridcells, we evaluated the best-fit slope for the portion of the data to the wetter side of the peak of the convex-up relationship.

We investigated sixteen hypothesized controllers of this slope (based on the literature cited in Sect. 1), all of which are represented explicitly or implicitly in PAWS+CLM: specific upslope area, gradient, variance of the gradient in each coarse-resolution gridcell, aspect, soil characteristics (porosity, clay content, conductivity), temporal mean evapotranspiration ($\overline{E_T}$ (W m^{-2})), temporal variance in evapotranspiration ($\hat{E_T}$ (W m^{-2})), bedrock topography, temporal mean groundwater depth ($\overline{G_w}$ (m)), temporal variance in groundwater depth ($\hat{G}_w$ (m)), elevation, mean surface roughness, variance in roughness, and stream drainage density. We used TopoToolbox (Schwanghart and Kuhn, 2010) to evaluate the topographic indices used in the analysis.

3 Results and discussion

3.1 Comparing model predictions to observations

PAWS+CLM has been extensively tested and demonstrated favorable comparisons with various observations from several basins (Niu et al., 2011; Niu and Phanikumar, 2012; Shen et al., 2013c; Shen and Phanikumar, 2010). In the Clinton River watershed, the model has been shown to satisfactorily reproduce streamflow observations both at the basin outlet and uncalibrated inner gages (Nash–Sutcliffe model efficiency coefficient ~ 0.65), spatially distributed water table depths ($R^2 = 0.66$), soil temperature, and MODIS observations of Leaf Area Index (LAI) and evapotranspiration (ET) (Shen et al., 2013c). In other basins, PAWS+CLM matched observed transient water table depths from a USGS monitoring well and water storage anomalies measured by the GRACE satellite (Niu and Phanikumar, 2012). Recent progress with the model includes comparisons with observed nitrogen and bacteria concentrations in the Great Lakes (Niu et al., 2011).

HESSD
11, 1967–2009, 2014

In addition to the comparisons described above, we compared simulated vs. observed soil moisture for a site in Romeo, MI from an Enviro-weather Automated Weather Station Network (Fig. 2). Since maintenance records indicated problems with the soil moisture sensor installation in 2008, we only show comparisons in 2009. The winter freeze-up at the beginning of 2009, shown as a period of very low soil moisture, was well captured by the model. The subsequent large variations due to freeze and thaw were also closely reproduced, with some over-estimation near the end of the freezing cycle (early April 2009). From May to November the model accurately predicted the mean, range of fluctuations ($0.25 \sim 0.34$), and general trend. However, toward the end of the year, the predicted freeze-up was not present in the observations.

3.2 Predicted mean moisture

The range and dynamics of predicted mean moisture at the coarse-resolution varied substantially across the watershed (Figs. 1 and 3). The western upland gridcells tended to be drier overall with the mean moisture increasing toward the east and south, which are lower elevation gridcells receiving both surface and sub-surface water inputs. The low precipitation inputs in 2003 had proportionally larger impacts in the wetter, eastern gridcells, resulting in up to 25 % decreases in mean saturation.

3.3 Relationships between soil moisture mean and higher-order moments

Using the 0–10 cm soil moisture predictions from the 220 m resolution simulation, we evaluated μ_θ, σ^2_θ, s_θ, and k_θ at every time point (daily) for each of the thirty-four 7040 m coarse-resolution gridcells (Fig. 4 shows representative transient profiles for one subregion over 90 d of the simulation). We used these temporally resolved values to build 1st, 2nd, and 3rd order best-fit polynomial relationships between the moments and μ_θ (Figs. 5, 7 and A1), with the 3rd order fits having generally the best predictive power and therefore applied in the remainder of our analysis. Overall, these surrogate models

HESSD
11, 1967–2009, 2014

accurately captured the relationships between μ_θ and σ^2_θ, s_θ, and k_θ, with mean R^2 values of 0.73, 0.74, and 0.75, respectively.

Different types of $\sigma^2_\theta \sim \mu_\theta$ relationships were predicted among the thirty-four coarse-resolution gridcells across the watershed. Some gridcells exhibited large, negative slopes with little scattering, e.g., #10, #17, #40, #41, indicating that soil moisture heterogeneity in these cells was strongly controlled by mean moisture, and that the variability was smallest on the wettest days. Some cells have much smaller slopes, e.g., #6, #7, #22 and #23, suggesting that their variability was less sensitive to mean moisture. These cells tended to have very small spatial variability throughout the year. Most gridcells with monotonic $\sigma^2_\theta \sim \mu_\theta$ relationships did not experience mean moisture below ~ 0.25. However, for some (e.g., gridcells #10, #17, #24), this monotonic, approximately linear relationship extended down to $\mu_\theta \sim 0.2$. We did not observe any gridcells with a purely upward $\sigma^2_\theta \sim \mu_\theta$ slope. On the other hand, about 20 % of the gridcells had convex up $\sigma^2_\theta \sim \mu_\theta$ relationships (e.g., gridcells #19, $26, #32 and #3). These gridcells primarily reside in the large topographic gradient in the middle of the watershed that alternates between recharge and discharge across the year (Salvucci and Entekhabi, 1995; Shen et al., 2013c) and correspond with relatively higher drainage densities (Fig. 6). The differences in these relationships indicate that at the 7040 m × 7040 m scale, the $\sigma^2_\theta \sim \mu_\theta$ relationships are determined locally, a finding consistent with that by Mascaro et al. (2010), where coefficients in a predictive formula for scaling exponents were related to local attributes.

For a particular coarse-resolution gridcell, the scattering of the $\sigma^2_\theta \sim \mu_\theta$ points around the polynomial fit, or departure from a deterministic function, can be attributed to different hydrologic processes that similarly affect the mean but differently affect the spatial heterogeneity. For example, homogeneous precipitation increases surface moisture evenly across the domain, and therefore decreases the variance. This homogenizing effect acts as the major driver that sets the negative slope in the $\sigma^2_\theta \sim \mu_\theta$ curves. However, an increase in regional groundwater flow would create spatial heterogeneity that adds to the variance. This effect is clear in the transition zones (e.g., gridcells #19, #26).

HESSD
11, 1967–2009, 2014

A floodwave that inundates riparian zones (which are represented in PAWS+CLM) would increase the mean soil moisture and spatial heterogeneity in the gridcell by increasing soil moisture only in the riparian zones. Gridcells that are further to the west have smaller σ_θ^2 ranges for particular values of μ_θ, and have soil moisture that are less impacted by exfiltration.

An alternative approach to define the coarse-grid sizes and shapes, as opposed to the fixed rectangular grids defined here, would be to identify zones that had, as close as possible, tight relationships between soil moisture mean and higher-order moments. This exercise could be performed within a search algorithm that starts with initial zonation defined by the features believed to be associated with such tight relationships, e.g., elevation, aspect, soil properties, vegetation properties, and stream drainage density. The algorithm should also consider the spatial scale of homogeneous precipitation in the region (Famiglietti et al., 2008), and ensure that the coarse-grid sizes are substantially smaller than this scale, although this criterion may be difficult to achieve.

As mentioned above, Famiglietti et al. (2008) used data from several ground-based measurement campaigns in the Southern Great Plains and Iowa to characterize relationships between μ_θ, σ_θ^2, and s_θ. They found convex up relationships between σ_θ^2 and μ_θ at 800 m and 50 km scales with a mean moisture range between ($\sim$ 0.05, 0.4), and fit an exponential relationship to the standard deviation: $\sigma_\theta = k_1 \mu_\theta \exp(-k_2 \mu_\theta)$. For the range of mean moisture we predicted in the Clinton Watershed ($\sim$ 0.2, 0.45) (i.e., a smaller range than in those observations), the overall monotonically declining trend in σ_θ^2 with μ_θ qualitatively matched the trend they reported (lower left panel of Fig. 5). There were, however, gridcells with higher variance that did not fit this pattern (i.e., #19, #26, #33). We calculated k_1 (1.3 ± 0.3) and k_2 ($7.1 \pm 1.$) across the 7040 m coarse-resolution gridcells and found a mean R^2 for all the gridcells of 0.48. These predicted values of k_1 and k_2 matched well those reported by Famiglietti et al. (2008) for their 1.6 km scale (1.2 and 7.1, respectively). We note also that the 3rd order polynomial fit explained more of the variance of the modeled relationships than did the

HESSD
11, 1967–2009, 2014

exponential relationship, but we are not aware of a mechanistically-based rationale for a choice of this relationship.

The relationships between μ_θ and s_θ also varied across the watershed (Fig. 7). For the gridcells toward the west (in the four western columns), which are typically drier than those to the east, s_θ was predominantly positive across the mean moisture range, implying a consistently right-skewed probability density function. The transition between positive and negative s_θ occurred in several of these gridcells at μ_θ of about 0.3–0.35 (#4, #10, #17). For the wetter gridcells to the east (column 5–7), the μ_θ distribution was predominantly left-skewed (i.e., $s_\theta < 0$), even though part of the μ_θ range was drier than the transition values for the gridcells farther to the west. For the sixth and seventh column (farthest east), μ_θ was predicted to be above 0.3 for the entire simulation period, and most of these gridcells (and those in the southern portion of column 5) showed a decreasing s_θ with increasing μ_θ. This pattern is consistent with the fact that there is a maximum μ_θ value possible (corresponding to fully saturated), and as more of the 220 m gridcells reach this level the probability density function becomes more left skewed.

Comparing our predictions (lower left panel of Fig. 7) to the 800 m and 50 km s_θ relationships with μ_θ reported in Famiglietti et al. (2008) indicates good qualitative agreement: a monotonic decrease from positive s_θ values between 0 and 1 at μ_θ of ~ 0.2 to a s_θ value of between about -1 and -2 at μ_θ of ~ 0.4. In our predictions, and somewhat visible in these observations, there is a divergence of s_θ values toward the wetter end of the μ_θ range. The best linear fit to these predictions had a slope of -13 and intercept of 4.2, which corresponded well to values inferred from their observations at the 1.6 km scale. However, the slope and intercepts inferred from their observations varied substantially (and inconsistently) across scale, making this comparison inconclusive.

The relationships between predicted k_θ and μ_θ (Fig. A1) can be divided into a few characteristic shapes: (1) monotonically increasing (e.g., #11, 27, 34, 41); (2) relatively constant (e.g., #18, 23); and (3) convex down (e.g., #13, 14, 20). To the extent that k_θ represents an index of "peakedness" in the moisture distribution, an increase in

HESSD
11, 1967–2009, 2014

k_θ with increasing mean moisture is consistent with the limit in the range occurring at full saturation, and with s_θ becoming more negative in this part of the range. The more strongly convex down shapes occur in gridcells where the mean soil moisture range extends to fully saturated, so the relationships that are more constant with μ_θ variations may simply be a result of that gridcell not experiencing periods with higher values of μ_θ.

Finally, we also tested our results against the theoretical predictions of Montaldo and Albertson (2003), who concluded that the time derivative of the root-zone soil moisture variance ($\frac{\partial \sigma_\theta^2}{\partial t}$) would increase as the covariance between soil moisture and infiltration increased, or decrease as the covariance between soil moisture and either drainage or transpiration increased. We tested these potential dependencies by comparing our predicted values of $\frac{\partial \sigma_\theta^2}{\partial t}$ to $\overline{\theta' K'}$, $\overline{\theta' q_r'}$, and $\overline{\theta' E'}$, where K is the soil hydraulic conductivity (which affects infiltration), q_r is the drainage flux, E is the evapotranspiration, the prime represents anomalies compared to the spatial mean of that variable, and the overbar represents a spatial average. We evaluated these relationships with daily, weekly, and monthly averaging periods using the model predictions and found very weak relationships. These results indicate that the creation and destruction of variance in a watershed model that represents a range of moisture redistribution mechanisms is more complex than can be represented by these inferred dependencies.

3.4 Predicted soil moisture pdf as a function of mean moisture

Because σ_θ^2, s_θ, and k_θ of the soil moisture field do not fully characterize the probability distribution function, we also examined the dependence of the proportion of high-resolution gridcells in each coarse-resolution gridcell occupying μ_θ bins (e.g., seven bins are shown in Fig. 8). The advantages of this binning approach are that it more fully represents the heterogeneity in μ_θ and allows visualization of variation within-coarse-resolution gridcells.

HESSD
11, 1967–2009, 2014

An interesting observation from these types of figures is that the coarse-resolution gridcells that have a clear convex up shape for variance vs. mean moisture have the peak of that distribution very close to where the 3rd and 4th quartile bands have equal representation (not shown). Thus, when the coarse-resolution gridcell has more of its fine-scale soil moisture mean values occupying the wettest quartile, the system variance begins to decline as mean moisture increases. In the gridcells that have a monotonically decreasing relationship, the transition between 3rd and 4th quartile mean moisture bands occurs to the drier end of the μ_θ range.

It is also interesting to note the different behavior of the wettest bin (the gray line). In many of the drier cells in the upland area (e.g., #23, #24, #10), this bin remains relatively constant across the μ_θ range. This pattern likely occurs because these regions have larger topographic variation and are effective at redistributing moisture, therefore preventing the wettest areas (or source areas (Dunne and Black, 1970; Frankenberger et al., 1999; Lyon et al., 2004)) from expanding in area. In many cells on the western plains (e.g., #27, #28, #40, #47), there appears to be a threshold soil moisture value, around 0.35, above which the wettest bin suddenly grows very rapidly as mean moisture increases. This appearance of criticality is due to the threshold effect of soil porosity and the flatter terrain. More research is required to explore the laws governing the shift of distributions and how they may be related to regional characteristics.

3.5 Relationships between soil moisture heterogeneity and system properties

As mentioned in Sect. 1, many of the convex up relationships reported in the literature appear to have a peak in this relationship at μ_θ of ~ 0.2, although that value is not universal (e.g., Rosenbaum et al., 2012). This transition point represents the transition between system properties (e.g., roughness, hydraulic conductivity) and fluxes (e.g., evapotranspiration) that tend to homogenize soil moisture vs. those that lead to more heterogeneity. For example, imagine a flat region with a distribution of plants of equal potential evapotranspiration but with drought tolerances that are different functions of soil moisture (Fig. A2 shows an example using CLM4.5's estimate of water stress on

HESSD
11, 1967–2009, 2014

photosynthesis (β_t) for soils with different sand composition). A precipitation event that occurs on a dry coarse-resolution gridcell would tend to alleviate the drought stress in a fraction of the plants, thereby leading to a higher heterogeneity in soil moisture (and therefore σ_θ^2). If the precipitation continued and μ_θ moved above the level where any of the plants were stressed, the now homogeneous evapotranspiration would tend to reduce σ_θ^2. As discussed in Sect. 2, many controllers of these tradeoffs have been inferred from observations, and include topographical features, evapotranspiration, and edaphic properties.

Because most of the coarse-resolution gridcells in our computational domain did not experience μ_θ below ~ 0.2, we investigated the relationship between σ_θ^2 and μ_θ over the range where σ_θ^2 decreases with increasing μ_θ. In our predictions, $\sim 80\,\%$ of the coarse-resolution gridcells were relatively well characterized by a linear fit with a negative slope. For the remaining $\sim 20\,\%$, we evaluated the best-fit slope for the portion of the data to the wetter side of the peak of the convex-up relationship.

Of the sixteen hypothesized controllers of this slope (m) that we investigated (see Sect. 2), six had independent linear best-fits with $R^2 > 0.05$: gradient (g; $R^2 = 0.07$), mean of evapotranspiration ($\overline{E_T}$ ($\mathrm{W\,m^{-2}}$); $R^2 = 0.16$), temporal mean of the spatial variance of evapotranspiration ($R^2 = 0.05$), porosity ($R^2 = 0.08$), mean of groundwater depth ($R^2 = 0.06$), and mean of stream density ($R^2 = 0.05$). Using a stepwise linear regression with these six variables and allowing for first order interactions, the best-fit model explained 59 % of the variance in m and had the form: $C_1 + C_2 g \overline{E_T}$, where C_1 and C_2 are constants. Thus, over the five years of simulation, the rate at which σ_θ^2 declined with increasing μ_θ was controlled primarily by the elevation gradient convolved with the temporal mean of evapotranspiration. In this relationship, increases in this product leads to less negative values of m (i.e., less sensitive response of σ_θ^2 to variations in μ_θ). The steeper and higher the evapotranspiration in the gridcell, the lower the response of soil moisture spatial heterogeneity to mean soil moisture. This conclusion is consistent with the ideas that (1) high evapotranspiration gridcells are more likely to be those with lower likelihood of partial water stress limitation and (2) the high gradient

HESSD
11, 1967–2009, 2014

systems more efficiently mix surface water thereby reducing soil moisture gradients. We note, however, that the complexity of the model applied here, with its representation of many factors that can influence soil moisture spatial heterogeneity, and the averaging period we applied (five years), may obscure important controllers of this relationship. Therefore, we believe the analysis described here is only a first step in using these types of models to evaluate these relationships. Carefully designed modeling experiments that isolate in turn the various processes are the next step toward improving understanding of the controls on these relationships.

3.6 Applying the simple surrogate models to predict fine-scale heterogeneity

We also evaluated whether the simple polynomial surrogate models can be used to predict dynamic variations in σ^2_θ, s_θ, and k_θ given variations in μ_θ. For this exercise, we used the first three years of the simulations to train the 3rd order polynomial surrogate model. We then applied those surrogates across the five years of simulation to evaluate estimates for σ^2_θ, s_θ, and k_θ within each coarse-resolution gridcell and compared those estimates to the moments calculated directly from the fine-resolution simulation.

The surrogate-estimated values of σ^2_θ over time corresponded well to those from the fine-scale solution, with an R^2 value of 0.78 and mean absolute bias of 0.00014 (Fig. 9). The estimates relatively accurately captured several of the dominant transients that occurred, including during the 2006 drought in, e.g., gridcells #26, #27, and #28. These gridcells span a μ_θ gradient from relatively drier to wetter, and that transition is apparent in the σ^2_θ gradient across these gridcells (from a value ~ 0.001 to ~ 0.006). The temporal dynamics during drying are also different between these gridcells; e.g., during 2006 the response in gridcell #26 is a reduction in σ^2_θ, while in gridcells #27 and #28 the response is an increase in σ^2_θ. This differential response occurred because gridcells #27 and #28 had μ_θ that was high enough before the drought that, even though they dried, remained to the right of the peak in the convex up relationship between σ^2_θ and

HESSD
11, 1967–2009, 2014

μ_θ. In contrast, gridcell #26 had a μ_θ value before the drought that was close to the peak in that relationship and the reduction in μ_θ therefore resulted in a reduction in σ^2_θ.

The surrogate-estimated values of s_θ over time corresponded well to those from the fine-scale solution, with an R^2 value of 0.74 and mean absolute bias of 0.11 (Fig. 10). The temporal variability in s_θ was largest in the coarse-resolution gridcells in the eastern (wetter) portion of the watershed, and in particular, during 2006 as the soils dried. During this period, for example, s_θ in gridcells #27 and #28 increased rapidly in Spring and then stabilized at a value near zero, indicating a relatively uniform distribution of μ_θ. Interestingly, the relatively drier gridcell #26 did not have as strong a response in s_θ, but all three gridcells stabilized at values indicating a more uniform μ_θ distribution.

The polynomial surrogate model for k_θ was less accurate than those for either s_θ or μ_θ, with an R^2 value of 0.51 and mean bias of 0.43 (Fig. A3). In contrast to the s_θ dynamics, k_θ was relatively temporally variable in both the western (e.g., gridcells #15, #29) and eastern portions of the watershed. In most years in many of the wetter southeastern gridcells there was a reduction in k_θ (i.e., a flattening of the μ_θ pdf) following the spring thaw followed by periodic increases associated with precipitation events. In contrast, during the 2006 dry period, the southeastern wetter gridcells showed a reduction that was sustained over the summer.

4 Limitations and future work

Many factors impact near-surface soil moisture heterogeneity in watersheds; characterizing this heterogeneity and its relationships with the mean moisture field, topographical features, vegetation, and climate forcing could improve regional to global-scale estimates of surface energy and greenhouse gas budgets. The approach we applied here, using a tested high-resolution numerical model, showed promise in this regard, yet a number of limitations remain for future work. For example, we did not consider the temporal pattern of the relationships, and therefore did not quantify the impacts of hysteresis on the relationships between the mean moisture field and higher-order

HESSD
11, 1967–2009, 2014

moments, as has been reported by Ivanov et al. (2010). The high-dimensional state space, especially the influence of vertical soil moisture profiles, also needs to be examined in detail. We also considered only one watershed over a relatively short (five-year) period. A longer study, covering several decades, would better capture the inter-annual range in precipitation and vegetation status (and therefore soil moisture) that the watershed experiences. Repeating the analyses described here for other watersheds with different topography, vegetation, bedrock features, soil properties, etc., could yield insights on the impacts these various properties have on soil moisture heterogeneity and its relationship with mean soil moisture. Such an analysis could also be used to test the extent to which relationships developed in one watershed could be used for other watersheds, and more specifically, for which watershed features such an extrapolation would be appropriate. We also note that soil moisture heterogeneity exists at scales much smaller than we simulated here (220 m), including down to the soil macropore scale, where the soil biogeochemical transformations that impact ecosystem function and climate occur. Developing modeling structures that account for, at some level, this wide range of scales will be important for consistently representing terrestrial ecosystem processes.

Finally, an important application of the relationships developed here would be to apply them with coarse-resolution simulations to substantially reduce computational costs for regional and global simulations. Comparisons between fine- and coarse-resolution simulations of a particular watershed have been used to transfer nonlinearity from microscale to mesoscale models via non-stationary effective parameters (Barrios and Frances, 2012). The approach we envision here would combine that type of model calibration with a cost function that includes a larger suite of observations, including the ability to capture the fine-scale predicted soil moisture heterogeneity and its relationship with mean moisture.

HESSD
11, 1967–2009, 2014

5 Summary and conclusions

We applied a watershed-scale hydrological model (PAWS+CLM) that has been previously tested in the Clinton River watershed in Michigan to investigate relationships between fine-scale near-surface soil moisture mean and spatial heterogeneity. We used fine-resolution (220 m) simulations to calculate statistical properties of soil moisture at a resolution 2^5 times coarser (~ 7 km), and then (1) developed and evaluated simple polynomial surrogate models relating soil moisture mean to its variance, skewness, and kurtosis during the non-frozen portion of five years; (2) applied those surrogates over the time period to evaluate their accuracy; and (3) investigated the relationship between the predicted soil moisture mean and variance and topographic and hydrological system properties.

The surrogate models accurately reproduced the relationships between the soil moisture mean and higher order moments (R^2 ~ 0.7–0.8). Driving the surrogate model with the mean coarse-resolution soil moisture predictions across the simulation period gave comparably accurate predictions for dynamic variance and skewness, and a less accurate (R^2 ~ 0.5) prediction of kurtosis.

In our predictions, and in many reported observations, there is typically a reduction in soil moisture variance with increasing mean past a particular intermediate value of the mean. Many possible controllers of this relationship have been hypothesized; in our predictions the approximately linear relationship was estimated (R^2 = 0.59) using only the elevation gradient convolved with the mean of evapotranspiration in the coarse-resolution gridcell. Increases in the elevation gradient and mean evapotranspiration each, and even more strongly in combination, caused a shallower slope in the soil moisture mean vs. variance relationships. An explanation for this pattern is that high evapotranspiration gridcells are more likely to be those with lower likelihood of partial water stress limitation and the high gradient gridcells more efficiently mix surface water. However, because we inferred these patterns from a full-complexity model with multiple interacting processes, we believe carefully designed modeling experiments that isolate

HESSD
11, 1967–2009, 2014

in turn the various processes will be helpful for better understanding the controls on these relationships. We conclude that these types of experiments can improve understanding of the causes of soil moisture heterogeneity across scales, and inform the types of observations required to more accurately represent what is often unresolved spatial heterogeneity in regional and global hydrological and biogeochemical models.

Acknowledgements. This research was supported by the Director, Office of Science, Office of Biological and Environmental Research of the US Department of Energy under Contract No. DE-AC02-05CH11231 as part of their Regional and Global Climate Modeling Program; and by the Next-Generation Ecosystem Experiments (NGEE Arctic) project, supported by the Office of Biological and Environmental Research in the DOE Office of Science under Contract No. DE-AC02-05CH11231. Shen was supported by Office of Biological and Environmental Research of the US Department of Energy under Contract No. DE-SC0010620. Cartographical help from Kuai Fang and Xinye Ji is appreciated.

References

Albertson, J. D. and Montaldo, N.: Temporal dynamics of soil moisture variability: 1. Theoretical basis, Water Resour. Res., 39, 1274, doi:10.1029/2002wr001616, 2003.

Arrigo, J. A. S. and Salvucci, G. D.: Investigation hydrologic scaling: observed effects of heterogeneity and nonlocal processes across hillslope, watershed, and regional scales, Water Resour. Res., 41, W11417, doi:10.1029/2005wr004032, 2005.

Barrios, M. and Frances, F.: Spatial scale effect on the upper soil effective parameters of a distributed hydrological model, Hydrol. Process., 26, 1022–1033, doi:10.1002/Hyp.8193, 2012.

Brocca, L., Morbidelli, R., Melone, F., and Moramarco, T.: Soil moisture spatial variability in experimental areas of central Italy, J. Hydrol., 333, 356–373, doi:10.1016/J.Jhydrol.2006.09.004, 2007.

Brocca, L., Melone, F., Moramarco, T., and Morbidelli, R.: Spatial-temporal variability of soil moisture and its estimation across scales, Water Resour. Res., 46, W02516, doi:10.1029/2009wr008016, 2010.

HESSD

11, 1967–2009, 2014

Brocca, L., Tullo, T., Melone, F., Moramarco, T., and Morbidelli, R.: Catchment scale soil moisture spatial-temporal variability, J. Hydrol., 422, 63–75, doi:10.1016/J.Jhydrol.2011.12.039, 2012.
Burt, T. P. and Pinay, G.: Linking hydrology and biogeochemistry in complex landscapes, Prog. Phys. Geog., 29, 297–316, doi:10.1191/0309133305pp450ra, 2005.
Chaplot, V. and Walter, C.: Subsurface topography to enhance the prediction of the spatial distribution of soil wetness, Hydrol. Process., 17, 2567–2580, doi:10.1002/Hyp.1273, 2003.
Choi, M. and Jacobs, J. M.: Spatial soil moisture scaling structure during Soil Moisture Experiment 2005, Hydrol. Process., 25, 926–932, doi:10.1002/Hyp.7877, 2011.
Crave, A. and GascuelOdoux, C.: The influence of topography on time and space distribution of soil surface water content, Hydrol. Process., 11, 203–210, doi:10.1002/(Sici)1099-1085(199702)11:2<203::Aid-Hyp432>3.0.Co;2-K, 1997.
Dai, Z. H., Trettin, C. C., Li, C. S., Li, H., Sun, G., and Amatya, D. M.: Effect of assessment scale on spatial and temporal variations in CH_4, CO_2, and N_2O fluxes in a forested wetland, Water Air Soil Poll., 223, 253–265, doi:10.1007/S11270-011-0855-0, 2012.
Das, N. N. and Mohanty, B. P.: Temporal dynamics of PSR-based soil moisture across spatial scales in an agricultural landscape during SMEX02: a wavelet approach, Remote Sens. Environ., 112, 522–534, doi:10.1016/J.Rse.2007.05.007, 2008.
Dunne, T. and Black, R. D.: Partial area contributions to storm runoff in a small New-England watershed, Water Resour. Res., 6, 1296–1311, doi:0.1029/Wr006i005p01296, 1970.
Famiglietti, J. S., Rudnicki, J. W., and Rodell, M.: Variability in surface moisture content along a hillslope transect: Rattlesnake Hill, Texas, J. Hydrol., 210, 259–281, doi:10.1016/S0022-1694(98)00187-5, 1998.
Famiglietti, J. S., Devereaux, J. A., Laymon, C. A., Tsegaye, T., Houser, P. R., Jackson, T. J., Graham, S. T., Rodell, M., and van Oevelen, P. J.: Ground-based investigation of soil moisture variability within remote sensing footprints during the Southern Great Plains 1997 (SGP97) Hydrology Experiment, Water Resour. Res., 35, 1839–1851, doi:10.1029/1999wr900047, 1999.
Famiglietti, J. S., Ryu, D. R., Berg, A. A., Rodell, M., and Jackson, T. J.: Field observations of soil moisture variability across scales, Water Resour. Res., 44, W01423, doi:10.1029/2006wr005804, 2008.

HESSD
11, 1967–2009, 2014

Frankenberger, J. R., Brooks, E. S., Walter, M. T., Walter, M. F., and Steenhuis, T. S.: A GIS-based variable source area hydrology model, Hydrol. Process., 13, 805–822, doi:10.1002/(Sici)1099-1085(19990430)13:6<805::Aid-Hyp754>3.0.Co;2-M, 1999.

Frei, S., Knorr, K. H., Peiffer, S., and Fleckenstein, J. H.: Surface micro-topography causes hot spots of biogeochemical activity in wetland systems: a virtual modeling experiment, J. Geophys. Res.-Biogeo., 117, G00n12, doi:10.1029/2012jg002012, 2012.

Gebremichael, M., Rigon, R., Bertoldi, G., and Over, T. M.: On the scaling characteristics of observed and simulated spatial soil moisture fields, Nonlinear Proc. Geoph., 16, 141–150, 2009.

Groffman, P. M., Hardy, J. P., Fisk, M. C., Fahey, T. J., and Driscoll, C. T.: Climate variation and soil carbon and nitrogen cycling processes in a northern Hardwood Forest, Ecosystems, 12, 927–943, doi:10.1007/S10021-009-9268-Y, 2009.

Hu, Z. L., Islam, S., and Cheng, Y. Z.: Statistical characterization of remotely sensed soil moisture images, Remote Sens. Environ., 61, 310–318, doi:10.1016/S0034-4257(97)89498-9, 1997.

Hupet, F. and Vanclooster, M.: Intraseasonal dynamics of soil moisture variability within a small agricultural maize cropped field, J. Hydrol., 261, 86–101, doi:10.1016/S0022-1694(02)00016-1, 2002.

Ivanov, V. Y., Vivoni, E. R., Bras, R. L., and Entekhabi, D.: Catchment hydrologic response with a fully distributed triangulated irregular network model, Water Resour. Res., 40, W11102, doi:10.1029/2004wr003218, 2004.

Ivanov, V. Y., Fatichi, S., Jenerette, G. D., Espeleta, J. F., Troch, P. A., and Huxman, T. E.: Hysteresis of soil moisture spatial heterogeneity and the “homogenizing” effect of vegetation, Water Resour. Res., 46, W09521, doi:10.1029/2009wr008611, 2010.

Jia, Y. W., Wang, H., Zhou, Z. H., and Qiu, Y. Q.: Development of the WEP-L distributed hydrological model and dynamic assessment of water resources in the Yellow River basin, J. Hydrol., 331, 606–629, doi:10.1016/J.Jhydrol.2006.06.006, 2006.

Joshi, C. and Mohanty, B. P.: Physical controls of near-surface soil moisture across varying spatial scales in an agricultural landscape during SMEX02, Water Resour. Res., 46, W12503, doi:10.1029/2010wr009152, 2010.

Koven, C. D., Riley, W. J., Subin, Z. M., Tang, J. Y., Torn, M. S., Collins, W. D., Bonan, G. B., Lawrence, D. M., and Swenson, S. C.: The effect of vertically resolved soil biogeochemistry

HESSD
11, 1967–2009, 2014

and alternate soil C and N models on C dynamics of CLM4, Biogeosciences, 10, 7109–7131, doi:10.5194/bg-10-7109-2013, 2013.
Lawrence, D. M., Oleson, K. W., Flanner, M. G., Thornton, P. E., Swenson, S. C., Lawrence, P. J., Zeng, X. B., Yang, Z. L., Levis, S., Sakaguchi, K., Bonan, G. B., and Slater, A. G.: Parameterization improvements and functional and structural advances in version 4 of the Community Land Model, J. Adv. Model. Earth Sy., 3, M03001, doi:10.1029/2011ms000045, 2011.
Lawrence, J. E. and Hornberger, G. M.: Soil moisture variability across climate zones, Geophys. Res. Lett., 34, L20402, doi:10.1029/2007gl031382, 2007.
Li, B. and Rodell, M.: Spatial variability and its scale dependency of observed and modeled soil moisture over different climate regions, Hydrol. Earth Syst. Sci., 17, 1177–1188, doi:10.5194/hess-17-1177-2013, 2013.
Li, Q., Unger, A. J. A., Sudicky, E. A., Kassenaar, D., Wexler, E. J., and Shikaze, S.: Simulating the multi-seasonal response of a large-scale watershed with a 3-D physically-based hydrologic model, J. Hydrol., 357, 317–336, doi:10.1016/J.Jhydrol.2008.05.024, 2008.
Lyon, S. W., Walter, M. T., Gerard-Marchant, P., and Steenhuis, T. S.: Using a topographic index to distribute variable source area runoff predicted with the SCS curve-number equation, Hydrol. Process., 18, 2757–2771, doi:10.1002/Hyp.1494, 2004.
Markstrom, S. L., Niswonger, R. G., Regan, R. S., Prudic, D. E., and Barlow, P. M.: GSFLOW-Coupled Ground-water and Surface-water FLOW model based on the integration of the Precipitation-Runoff Modeling System (PRMS) and the Modular Ground-Water Flow Model (MODFLOW-2005), US Geological Survey, Reston, VA, USA, 240 pp., 2008.
Mascaro, G., Vivoni, E. R., and Deidda, R.: Downscaling soil moisture in the southern Great Plains through a calibrated multifractal model for land surface modeling applications, Water Resour. Res., 46, W08546, doi:10.1029/2009wr008855, 2010.
Mascaro, G., Vivoni, E. R., and Deidda, R.: Soil moisture downscaling across climate regions and its emergent properties, J. Geophys. Res.-Atmos., 116, D22114, doi:10.1029/2011jd016231, 2011.
Maxwell, R. M.: Infiltration in arid environments: spatial patterns between subsurface heterogeneity and water-energy balances, Vadose Zone J., 9, 970–983, doi:10.2136/Vzj2010.0014, 2010.
Maxwell, R. M., Putti, M., Meyerhoff, S., J.- Delfs,O., Ferguson, I. M., Ivanov, V., Kim, J., O.Kolditz, Kollet, S. J., Kumar, M., Paniconi, C., Park, Y.-J., Phanikumar, M. S.,

HESSD
11, 1967–2009, 2014

Sudicky, E., and Sulis, M.: Surface-subsurface model intercomparison: a first set of benchmark results to diagnose integrated hydrology and feedbacks, paper presented at EGU General Assembly, AGU, Vienna, Austria, 22–27 April, 2012.
McClain, M. E., Boyer, E. W., Dent, C. L., Gergel, S. E., Grimm, N. B., Groffman, P. M., Hart, S. C., Harvey, J. W., Johnston, C. A., Mayorga, E., McDowell, W. H., and Pinay, G.: Biogeochemical hot spots and hot moments at the interface of terrestrial and aquatic ecosystems, Ecosystems, 6, 301–312, doi:10.1007/S10021-003-0161-9, 2003.
McMichael, C. E., Hope, A. S., and Loaiciga, H. A.: Distributed hydrological modelling in California semi-arid shrublands: MIKE SHE model calibration and uncertainty estimation, J. Hydrol., 317, 307–324, doi:10.1016/J.Jhydrol.2005.05.023, 2006.
Merot, P., Ezzahar, B., Walter, C., and Aurousseau, P.: Mapping waterlogging of soils using digital terrain models, Hydrol. Process., 9, 27–34, doi:10.1002/Hyp.3360090104, 1995.
Miguez-Macho, G. and Fan, Y.: The role of groundwater in the Amazon water cycle: 1. Influence on seasonal streamflow, flooding and wetlands, J. Geophys. Res.-Atmos., 117, D15113, doi:10.1029/2012jd017539, 2012.
Montaldo, N. and Albertson, J. D.: Temporal dynamics of soil moisture variability: 2. Implications for land surface models, Water Resour. Res., 39, 1275, doi:10.1029/2002wr001618, 2003.
Moore, I. D., Burch, G. J., and Mackenzie, D. H.: Topographic effects on the distribution of surface soil-water and the location of ephemeral gullies, T. Asae., 31, 1098–1107, 1988.
Moore, I. D., Norton, T. W., and Williams, J. E.: Modeling environmental heterogeneity in forested landscapes, J. Hydrol., 150, 717–747, doi:10.1016/0022-1694(93)90133-T, 1993.
Niu, G. Y., Paniconi, C., Troch, P. A., Scott, R. L., Durcik, M., Zeng, X., Huxman, T. E., and Goodrich, D. C.: An integrated modelling framework of catchment-scale ecohydrological processes: 1. Model description and tests over an energy-limited watershed, Ecohydrology, submitted, 2013.
Niu, J. and Phanikumar, M. S.: Quantifying fluxes of chemical and biological species in Great Lakes watersheds: a reactive transport modeling framework, paper presented at American Geophysical Union Annual Fall Meeting, San Francisco, CA, 2012.
Niu, J., Shen, C., and Phanikumar, M. S.: Quantifying water budgets in regional Great Lakes watersheds using a process-based, distributed hydrologic model, paper presented at International Association for Great Lakes Research Annual Conference, Duluth, MN, 30 May–3 June 2011, 2011.

HESSD
11, 1967–2009, 2014

Nykanen, D. K. and Foufoula-Georgiou, E.: Soil moisture variability and scale-dependency of nonlinear parameterizations in coupled land-atmosphere models, Adv. Water Resour., 24, 1143–1157, doi:10.1016/S0309-1708(01)00046-X, 2001.

Pan, F. and Peters-Lidard, C. D.: On the relationship between mean and variance of soil moisture fields, J. Am. Water Resour. As., 44, 235–242, doi:10.1111/J.1752-1688.2007.00150.X, 2008.

Park, S. J. and van de Giesen, N.: Soil-landscape delineation to define spatial sampling domains for hillslope hydrology, J. Hydrol., 295, 28–46, doi:10.1016/J.Jhydrol.2004.02.022, 2004.

Qiu, Y., Fu, B. J., Wang, J., and Chen, L. D.: Soil moisture variation in relation to topography and land use in a hillslope catchment of the Loess Plateau, China, J. Hydrol., 240, 243–263, doi:10.1016/S0022-1694(00)00362-0, 2001.

Qu, Y. Z. and Duffy, C. J.: A semidiscrete finite volume formulation for multiprocess watershed simulation, Water Resour. Res., 43, W08419, doi:10.1029/2006wr005752, 2007.

Rigon, R., Bertoldi, G., and Over, T. M.: GEOtop: A distributed hydrological model with coupled water and energy budgets, J. Hydrometeorol., 7, 371–388, doi:10.1175/Jhm497.1, 2006.

Rodriguez-Iturbe, I., Vogel, G. K., Rigon, R., Entekhabi, D., Castelli, F., and Rinaldo, A.: On the spatial-organization of soil-moisture fields, Geophys. Res. Lett., 22, 2757–2760, doi:10.1029/95gl02779, 1995.

Rosenbaum, U., Bogena, H. R., Herbst, M., Huisman, J. A., Peterson, T. J., Weuthen, A., Western, A. W., and Vereecken, H.: Seasonal and event dynamics of spatial soil moisture patterns at the small catchment scale, Water Resour. Res., 48, W10544, doi:10.1029/2011wr011518, 2012.

Ryu, D. and Famiglietti, J. S.: Characterization of footprint-scale surface soil moisture variability using Gaussian and beta distribution functions during the Southern Great Plains 1997 (SGP97) hydrology experiment, Water Resour. Res., 41, W12433, doi:10.1029/2004wr003835, 2005.

Salvucci, G. D. and Entekhabi, D.: Hillslope and climatic controls on hydrologic fluxes, Water Resour. Res., 31, 1725–1739, doi:10.1029/95wr00057, 1995.

Schwanghart, W. and Kuhn, N. J.: TopoToolbox: A set of Matlab functions for topographic analysis, Environ. Modell. Softw., 25, 770–781, doi:10.1016/J.Envsoft.2009.12.002, 2010.

Seyfried, M.: Spatial variability constraints to modeling soil water at different scales, Geoderma, 85, 231–254, doi:10.1016/S0016-7061(98)00022-6, 1998.

HESSD
11, 1967–2009, 2014

Shen, C.: A process-based distributed hydrologic model and its application to a Michigan watershed, Michigan State University, East Lansing, MI, 270 pp., 2009.
Shen, C. P. and Phanikumar, M. S.: A process-based, distributed hydrologic model based on a large-scale method for surface-subsurface coupling, Adv. Water Resour., 33, 1524–1541, doi:10.1016/J.Advwatres.2010.09.002, 2010.
Shen, C., Fang, K., Salve, R., Godfrey, P., and Ludwig, N.: Assessing the importance of groundwater flow in ecosystem functioning using a process-based surface-subsurface model, paper presented at International Workshop on Observation and Modeling of Ecohydrological Processes in Inland River Basins: A Vision for Transformative Science, Beijing, China, 5–9 July 2013, 2013a.
Shen, C., Niu, J., and Phanikumar, M. S.: PAWS+CLM: a computationally efficient framework for linking hydrologic and ecosystem processes with GIS data integration capabilities, Hydrol. Earth Syst. Sci., in review, 2013b.
Shen, C., Niu, J., and Phanikumar, M. S.: Evaluating controls on coupled hydrologic and vegetation dynamics in a humid continental climate watershed using a subsurface – land surface process model, Water Resour. Res., 49, 2552–2572, doi:10.1002/wrcr.20189, 2013c.
Subin, Z. M., Riley, W. J., Jin, J., Christianson, D. S., Torn, M. S., and Kueppers, L. M.: Ecosystem feedbacks to climate change in California: development, testing, and analysis using a coupled regional atmosphere and land surface model (WRF3-CLM3.5), Earth Interact., 15, 15, doi:10.1175/2010ei331.1, 2011.
Tague, C., Band, L., Kenworthy, S., and Tenebaum, D.: Plot- and watershed-scale soil moisture variability in a humid Piedmont watershed, Water Resour. Res., 46, W12541, doi:10.1029/2009wr008078, 2010.
Tang, J. Y., Riley, W. J., Koven, C. D., and Subin, Z. M.: CLM4-BeTR, a generic biogeochemical transport and reaction module for CLM4: model development, evaluation, and application, Geosci. Model Dev., 6, 127–140, doi:10.5194/gmd-6-127-2013, 2013.
Teuling, A. J. and Troch, P. A.: Improved understanding of soil moisture variability dynamics, Geophys. Res. Lett., 32, L05404, doi:10.1029/2004gl021935, 2005.
Teuling, A. J., Hupet, F., Uijlenhoet, R., and Troch, P. A.: Climate variability effects on spatial soil moisture dynamics, Geophys. Res. Lett., 34, L06406, doi:10.1029/2006gl029080, 2007.
Vereecken, H., Kamai, T., Harter, T., Kasteel, R., Hopmans, J., and Vanderborght, J.: Explaining soil moisture variability as a function of mean soil moisture: a stochastic unsaturated flow perspective, Geophys. Res. Lett., 34, L22402, doi:10.1029/2007gl031813, 2007.

HESSD
11, 1967–2009, 2014

Vivoni, E. R., Entekhabi, D., Bras, R. L., and Ivanov, V. Y.: Controls on runoff generation and scale-dependence in a distributed hydrologic model, Hydrol. Earth Syst. Sci., 11, 1683–1701, doi:10.5194/hess-11-1683-2007, 2007.

Weill, S., Mazzia, A., Putti, M., and Paniconi, C.: Coupling water flow and solute transport into a physically-based surface-subsurface hydrological model, Adv. Water Resour., 34, 128–136, doi:10.1016/J.Advwatres.2010.10.001, 2011.

Western, A. W., Grayson, R. B., Bloschl, G., Willgoose, G. R., and McMahon, T. A.: Observed spatial organization of soil moisture and its relation to terrain indices, Water Resour. Res., 35, 797–810, doi:10.1029/1998wr900065, 1999.

Williams, A. G., Ternan, J. L., Fitzjohn, C., de Alba, S., and Perez-Gonzalez, A.: Soil moisture variability and land use in a seasonally arid environment, Hydrol. Process., 17, 225–235, doi:10.1002/Hyp.1120, 2003.

Wilson, D. J., Western, A. W., and Grayson, R. B.: Identifying and quantifying sources of variability in temporal and spatial soil moisture observations, Water Resour. Res., 40, W02507, doi:10.1029/2003wr002306, 2004.

Wood, E. F.: Effects of soil moisture aggregation on surface evaporative fluxes, J. Hydrol., 190, 397–412, doi:10.1016/S0022-1694(96)03135-6, 1997.

Wood, E. F.: Scale analyses for land-surface hydrology, in: Scale Dependence and Scale Invariance in Hydrology, edited by: Sposito, G., Cambridge University Press, Cambridge, UK, 1–29, 1998.

Wood, E. F., Roundy, J. K., Troy, T. J., van Beek, L. P. H., Bierkens, M. F. P., Blyth, E., de Roo, A., Doll, P., Ek, M., Famiglietti, J., Gochis, D., van de Giesen, N., Houser, P., Jaffe, P. R., Kollet, S., Lehner, B., Lettenmaier, D. P., Peters-Lidard, C., Sivapalan, M., Sheffield, J., Wade, A., and Whitehead, P.: Hyperresolution global land surface modeling: Meeting a grand challenge for monitoring Earth's terrestrial water, Water Resour. Res., 47, W05301, doi:10.1029/2010wr010090, 2011.

Zhang, Y., Sachs, T., Li, C. S., and Boike, J.: Upscaling methane fluxes from closed chambers to eddy covariance based on a permafrost biogeochemistry integrated model, Glob. Change Biol., 18, 1428–1440, doi:10.1111/J.1365-2486.2011.02587.X, 2012.

HESSD
11, 1967–2009, 2014

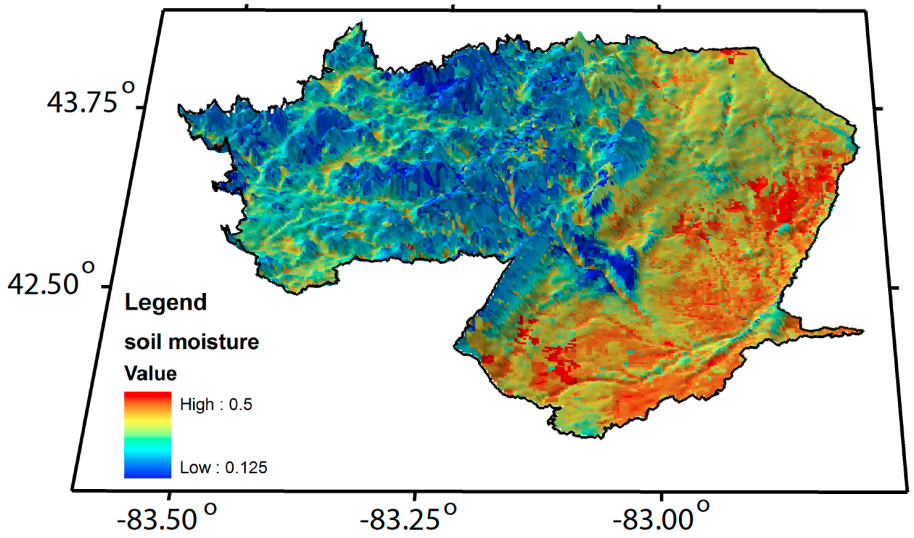

Fig. 1. Topography and predicted 2004–2008 temporal average soil moisture of the Clinton River watershed (the black line outlines the watershed). The 3-D elevation and shade represents the digital elevation model, which is enhanced by a 1 : 50 ratio, and the color represents the average soil moisture.

HESSD
11, 1967–2009, 2014

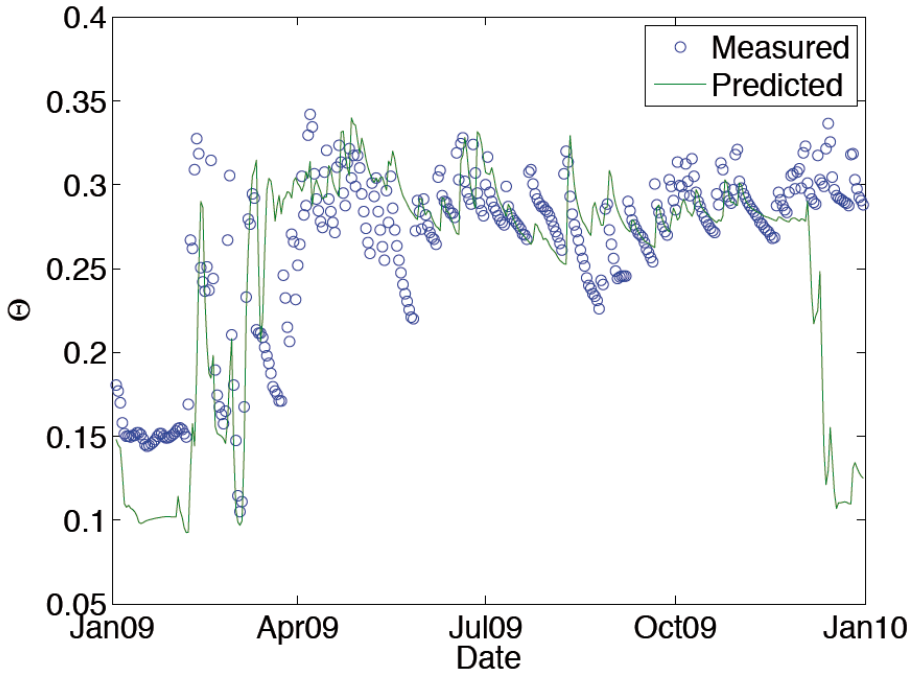

Fig. 2. Comparison between 220 m resolution predicted and measured soil moisture for a site in Romeo, MI. The large differences in December 2009 are caused by the model predicting freezing in the top 10 cm of soil, while the observations suggest unfrozen conditions.

HESSD
11, 1967–2009, 2014

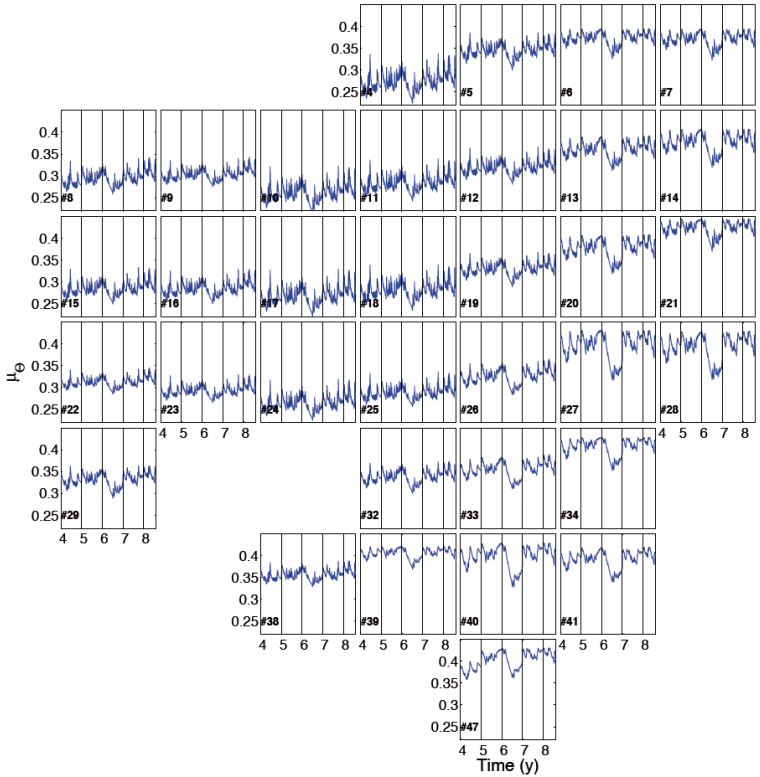

Fig. 3. Fine-resolution (220 m) simulated 0–10 cm soil moisture mean (μ_θ). The individual plots are distributed in the same pattern as the coarse-resolution gridcell they represent in the watershed (see watershed boundary in Fig. 1).

HESSD
11, 1967–2009, 2014

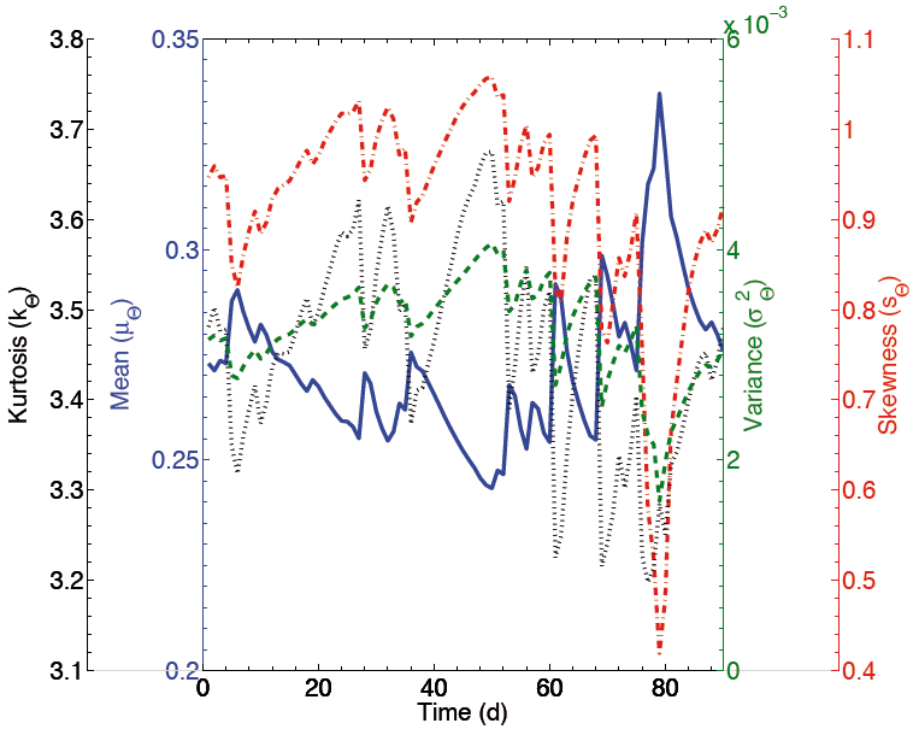

Fig. 4. Example 90 day soil moisture mean (μ_θ; blue solid line), variance (σ_θ; green dashed line), skewness (s_θ; red dashed-dotted line), and kurtosis (κ_θ; black dotted line) for gridcell #26.

HESSD
11, 1967–2009, 2014

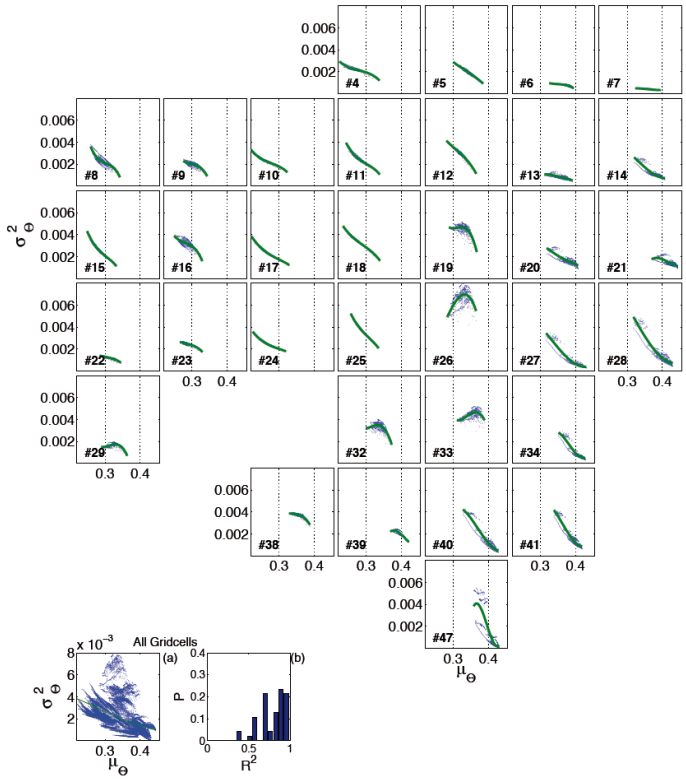

Fig. 5. In each subplot (except for the two in the bottom left hand corner), soil moisture variance (σ_θ^2) is plotted vs. mean (μ_θ) for that coarse-resolution gridcell based on the fine-resolution (220 m) model predictions (blue dots) and the best-fit 3rd order polynomial fits (green line). The individual 7040 m coarse-resolution gridcells are placed in their relative position in the watershed. Bottom left hand corner: **(a)** Soil moisture variance (σ_θ^2) vs. mean (μ_θ) for all gridcells combined; **(b)** the pdf of R^2 values referenced to the polynomial fit from each coarse-resolution gridcell.

HESSD
11, 1967–2009, 2014

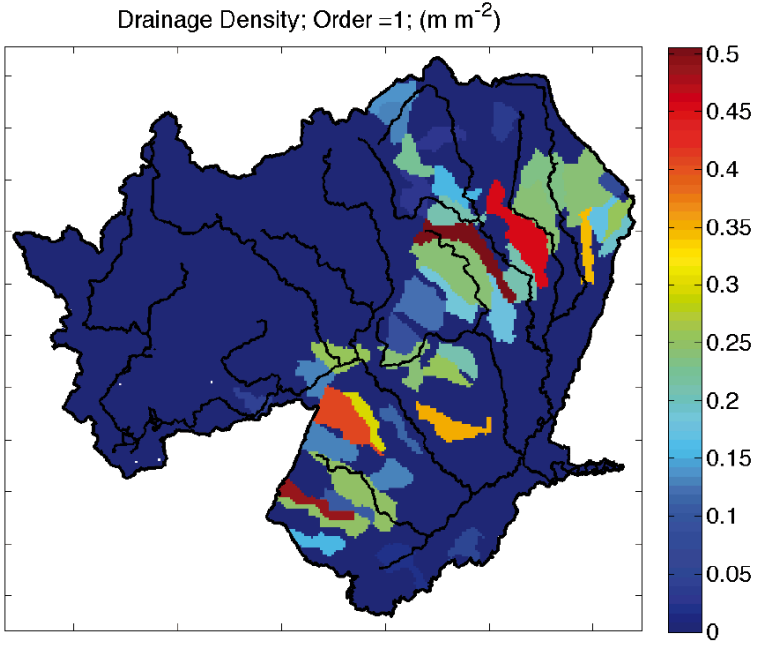

Fig. 6. Drainage density (length of streams per area) for streams of order 1 and higher. Areas with clear convex up shapes for soil moisture variance versus mean tend to be in gridcells with higher drainage density.

HESSD
11, 1967–2009, 2014

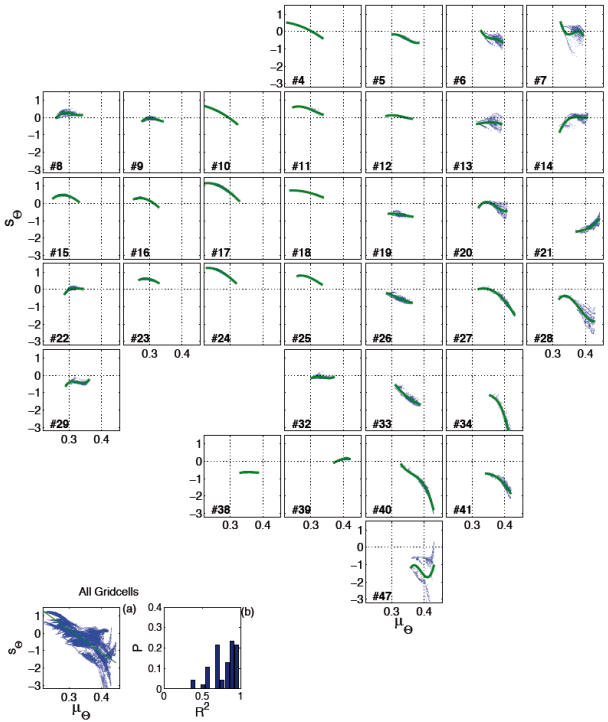

Fig. 7. In each subplot (except for the two in the bottom left hand corner), soil moisture skewness (s_θ) is plotted vs. mean (μ_θ) for that coarse-resolution gridcell based on the fine-resolution (220 m) model predictions (blue dots) and the best-fit 3rd order polynomial fits (green line). The individual 7040 m coarse-resolution gridcells are placed in their relative position in the watershed. Bottom left hand corner: **(a)** Soil moisture skewness (s_θ) vs. mean (μ_θ) for all gridcells combined; **(b)** the pdf of R^2 values referenced to the polynomial fit from each coarse-resolution gridcell.

HESSD
11, 1967–2009, 2014

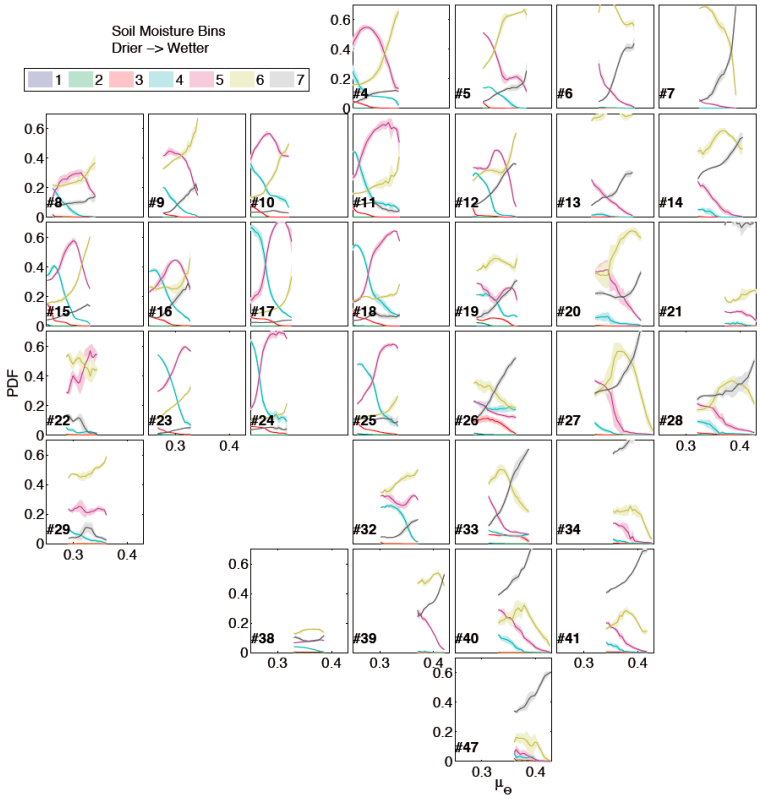

Fig. 8. Relationships between mean coarse-resolution gridcell soil moisture (μ_θ) and the proportion of the gridcell in each of ten moisture bins (the wettest seven bins are shown) that span that coarse-resolution gridcell's μ_θ range over the five years of simulation. The individual 7040 m coarse-resolution gridcells are placed in their relative position in the watershed.

HESSD
11, 1967–2009, 2014

Fine-scale simulations

W. J. Riley and C. Shen

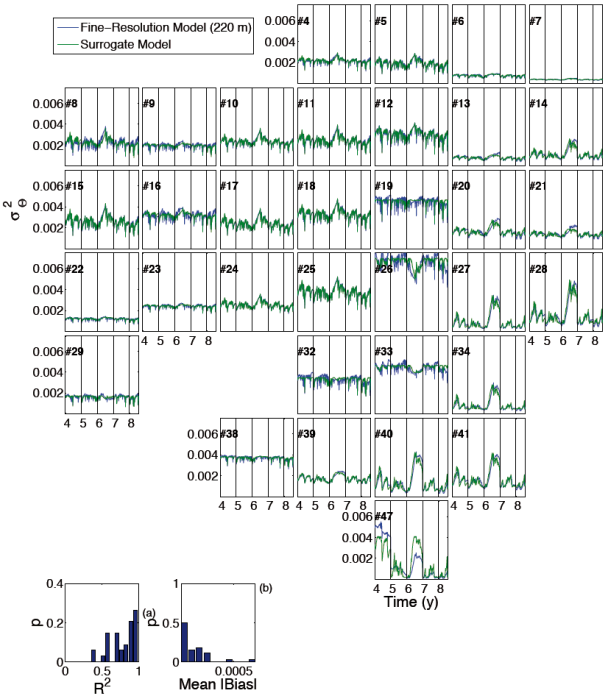

Fig. 9. Comparison over time between the fine-resolution (220 m) simulated soil moisture variance (σ^2_θ) and that predicted by the surrogate model using the mean of the fine-resolution soil moisture (μ_θ). The individual 7040 m coarse-resolution gridcells are placed in their relative position in the watershed. Bottom left hand corner: **(a)** the pdf of R^2 values between the surrogate model and fine-resolution model predictions of soil moisture variance across all the coarse-resolution gridcells; **(b)** mean absolute bias between the surrogate and fine-model predictions of soil moisture variance across all the coarse-resolution gridcells.

HESSD
11, 1967–2009, 2014

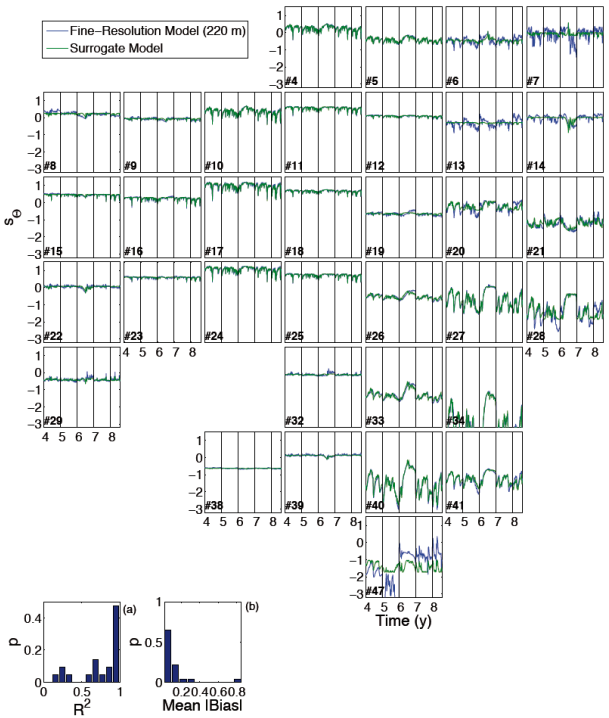

Fig. 10. Comparison over time between the fine-resolution (220 m) simulated soil moisture skewness (s_θ) and that predicted by the surrogate model using the mean of the fine-resolution soil moisture (μ_θ). The individual 7040 m coarse-resolution gridcells are placed in their relative position in the watershed. Bottom left hand corner: **(a)** the pdf of R^2 values between the surrogate model and fine-resolution model predictions of soil moisture skewness across all the coarse-resolution gridcells; **(b)** mean absolute bias between the surrogate and fine-model predictions of soil moisture skewness across all the coarse-resolution gridcells.

HESSD
11, 1967–2009, 2014

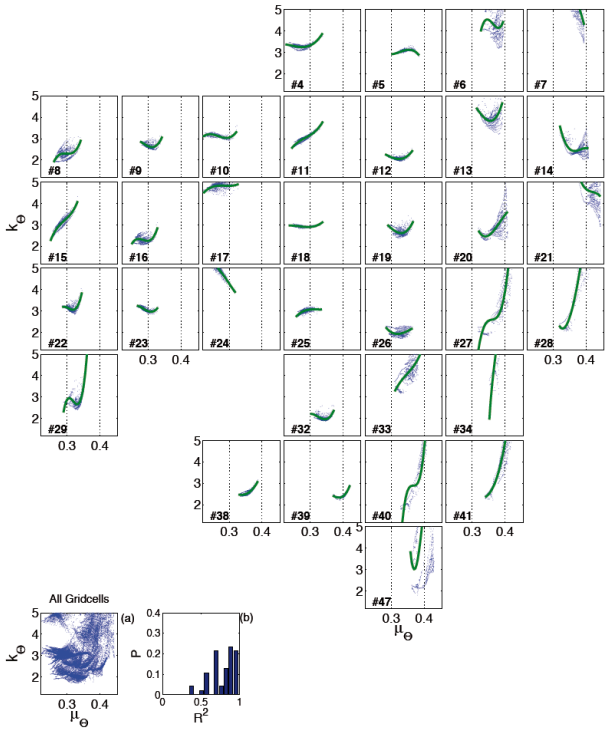

Fig. A1. In each subplot (except for the two in the bottom left hand corner), soil moisture kurtosis (κ_θ) is plotted vs. mean (μ_θ) for that coarse-resolution gridcell based on the fine-resolution (220 m) model predictions (blue dots) and the best-fit 3rd order polynomial fits (green line). The individual 7040 m coarse-resolution gridcells are placed in their relative position in the watershed. Bottom left hand corner: **(a)** Soil moisture kurtosis (κ_θ) vs. mean (μ_θ) for all gridcells combined; **(b)** the pdf of R^2 values referenced to the polynomial fit from each coarse-resolution gridcell.

HESSD
11, 1967–2009, 2014

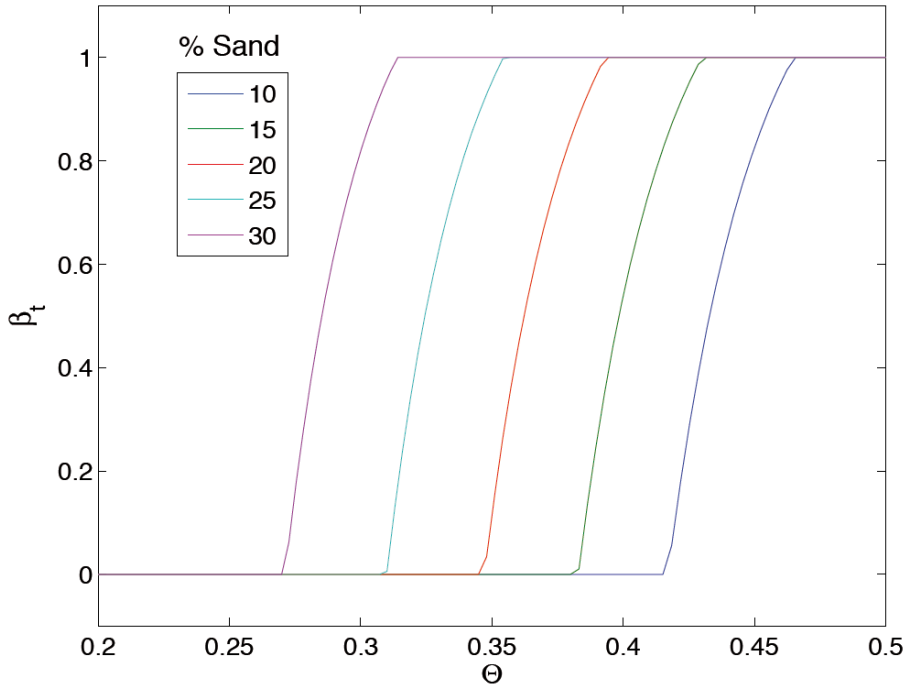

Fig. A2. The water stress term on photosynthesis applied in CLM4 as a function of percent sand of the soil.

HESSD
11, 1967–2009, 2014

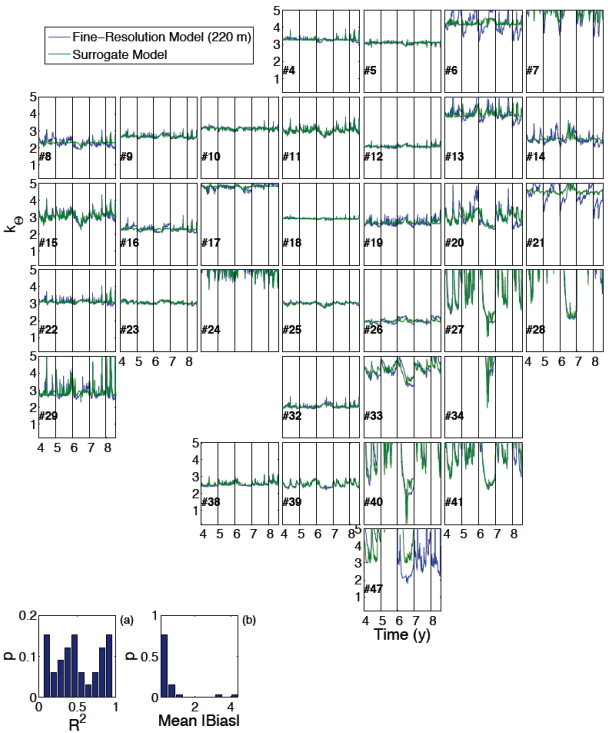

Fig. A3. Comparison over time between the fine-resolution (220 m) simulated soil moisture kurtosis (κ) and that predicted by the surrogate model using the mean of the fine-resolution soil moisture (μ_θ). The individual 7040 m coarse-resolution gridcells are placed in their relative position in the watershed. Bottom left hand corner: **(a)** the pdf of R^2 values between the surrogate model and fine-resolution model predictions of soil moisture kurtosis across all the coarse-resolution gridcells; **(b)** mean absolute bias between the surrogate and fine-model predictions of soil moisture kurtosis across all the coarse-resolution gridcells.

HESSD
11, 1967–2009, 2014